

Article

Preparation and Physical Properties of High-Belite Sulphoaluminate Cement-Based Foam Concrete Using an Orthogonal Test

Chao Liu ¹, Jianlin Luo ^{1,2,3,*} , Qiuyi Li ^{2,4,*}, Song Gao ^{1,2}, Zuquan Jin ^{1,2}, Shaochun Li ^{1,2}, Peng Zhang ^{1,2}  and Shuaichao Chen ¹

¹ School of Civil Engineering, Qingdao University of Technology, Qingdao 266033, China; alexlc@163.com (C.L.); gaosong727@126.com (S.G.); jinzuquan@126.com (Z.J.); 15063016520@126.com (S.L.); zhp0221@163.com (P.Z.); 17853245963@163.com (S.C.)

² Collaborative Innovation Center of Engineering Construction and Safety in Shandong Blue Economic Zone, Qingdao University of Technology, Qingdao 266033, China

³ Center for Infrastructure Engineering, School of Computing, Engineering and Mathematics, Western Sydney University, Sydney, NSW 2751, Australia

⁴ School of Architecture Engineering, Qingdao Agricultural University, Qingdao 266109, China

* Correspondence: lawjanelim@qut.edu.cn or j.luo@westernsydney.edu.au (J.L.); lqyyxn@163.com (Q.L.); Tel.: +86-532-8507-1605 (J.L.); 86-532-8507-1218 (Q.L.)

Received: 27 February 2019; Accepted: 17 March 2019; Published: 25 March 2019



Abstract: Prefabricated building development increasingly requires foam concrete (FC) insulation panels with low dry density (ρ_d), low thermal conductivity coefficient (k_c), and a certain compressive strength (f_{cu}). Here, the foam properties of a composite foaming agent with different dilution ratios were studied first, high-belite sulphoaluminate cement (HBSC)-based FCs (HBFCs) with 16 groups of orthogonal mix proportions were subsequently fabricated by a pre-foaming method, and physical properties (ρ_d , f_{cu} , and k_c) of the cured HBFC were characterized in tandem with microstructures. The optimum mix ratios for ρ_d , f_{cu} , and k_c properties were obtained by the range analysis and variance analysis, and the final optimization verification and economic cost of HBFC was also carried out. Orthogonal results show that foam produced by the foaming agent at a dilution ratio of 1:30 can meet the requirements of foam properties for HBFC, with the 1 h bleeding volume, 1 h settling distance, foamability, and foam density being 65.1 ± 3.5 mL, 8.0 ± 0.4 mm, 27.9 ± 0.9 times, and 45.0 ± 1.4 kg/m³, respectively. The increase of fly ash (FA) and foam dosage can effectively reduce the k_c of the cured HBFC, but also leads to the decrease of f_{cu} due to the increase in mean pore size and the connected pore amount, and the decline of pore uniformity and pore wall strength. When the dosage of FA, water, foam, and the naphthalene-based superplasticizer of the binder is 20 wt%, 0.50, 16.5 wt%, and 0.6 wt%, the cured HBFC with ρ_d of 293.5 ± 4.9 kg/m³, f_{cu} of 0.58 ± 0.02 MPa and k_c of 0.09234 ± 0.00142 W/m·k is achieved. In addition, the cost of HBFC is only 39.5 \$/m³, which is 5.2 \$ lower than that of ordinary Portland cement (OPC)-based FC. If the surface of the optimized HBFC is further treated with water repellent, it will completely meet the requirements for a prefabricated ultra-light insulation panel.

Keywords: foam concrete; high-belite sulphoaluminate cement; dilution ratio; dry density; compressive strength; thermal insulation; microstructure

1. Introduction

Since ‘sustainability’ was widely adopted as a key criterion for the assessment of construction materials and buildings [1–3], researchers around the world have realized the growing demand

for lightweight, economical, easy-to-use, and environmentally sustainable building materials in the future [4–8]. Foam concrete (FC) products with low self-weight, high specific strength, and excellent thermal insulation performance become very attractive in the application of prefabricated building panels [7,9]. FC products can effectively reduce dead loads on the structure and foundation, contribute to energy conservation, and lower the labor cost during construction [10,11]. Nowadays, FC has been commonly used in construction applications in different countries such as Germany, UK, Philippines, Turkey, Thailand, and China [12,13].

FC is generally produced with cement, filler, water, and a liquid chemical under controlled conditions, and the liquid chemical can be diluted by water and aerated to foaming [14–22]. Although the dry density (ρ_d) and thermal conductivity coefficient (k_c) of FC is lower than that of ordinary concrete, its insufficiency of high porosity, multiple connected pores, and low strength limits its widespread development. Recently, a lot of research has been done to further improve the performance of FC [23–31]. Kearsley and Wainwright found that replacing cement with a high content of fly ash (FA) could enhance the late strength of FC [26]. Khan et al. found that polypropylene fiber (PP) could increase the flexural strength (f_b) and tensile strength (f_t) of FC, but it had no effect on compressive strength (f_{cu}), while basalt fiber could greatly increase f_{cu} , f_b , and f_t of FC, which was better than PP [27]. Luo et al. reported that adding multi-walled carbon nanotubes (CNTs) to FC could improve pore structure and reduce average pore size [28]. Yakovlev et al. found that adding CNTs to FC could significantly increase its f_{cu} and effectively improve its heat insulation [29]. Szelag introduced CNTs dispersion and sodium dodecyl sulfate (SDS) into the cement slurry and found that a large amount of foam was generated after fast stirring due to the foaming characteristics of SDS, which greatly reduced the density, and concluded that CNTs reinforced cement paste with SDS was expected to be used in the production of lightweight concrete [30]. Sun et al. explored the effects of a synthetic surfactant, plant surfactant, and animal glue/blood-based surfactant on the properties of FC and found that FC prepared by the synthetic surfactant had a higher f_{cu} and smaller shrinkage [31].

From the findings of the above studies, the performance of FC is still does not meet the requirements for a prefabricated insulation wall. In addition, due to the slow setting feature of ordinary Portland cement (OPC), it is difficult to match the defoaming time of the foam [3,17], frequently resulting in the collapse of the FC. Moreover, the early-stage strength of FC prepared with OPC increases slowly, which is not conducive to its application in the prefabricated industry and affects the engineering efficiency [32]. Unlike sulphoaluminate cement (SAC), which uses a lot of expensive bauxite, high-belite sulphoaluminate cement (HBSC) can be mostly calcined by construction and industrial waste, which is consistent with the concept of sustainability [33–39]. HBSC has many advantages, such as fast setting, fast hardening, early strength, high strength, small expansion, low dry shrinkage, anti-freezing, anti-permeability, anti-corrosion, and so on [36]. Indeed, nowadays HBSC is widely used, allowing that HBSC-based FC (HBFC) has better thermal insulation performance than ordinary concrete and can be used for insulation panels to realize the energy-saving efficiency of buildings [20].

HBFC can be used to control the stability of bubbles in FC, and high strengths can be attained in the initial stages of curing. Therefore, the preparation of FC with HBSC is conducive to the optimization of properties.

There are two techniques that could be used in the FC process; the pre-foaming method and mix-foaming method [40–43]. The pre-foaming method is to make the foam before mixing it with slurry and, after mixing evenly, the FC slurry is poured into the mold to form an FC product. The mix-foaming method is to prepare a slurry containing a foaming agent first, then pre-cast the slurry and complete the foaming during incubation [36]. The fresh FC prepared by the pre-foaming method has good fluidity and can be pumped to a long distance, which meets the prefabricated process, while the mix-foaming method is generally not used for pumping and just for on-site pouring.

Orthogonal experiments can be used to effectively explore the relative importance of various factors on the performance of HBSC-based FC (HBFC). The optimum level of different factors can be

determined by orthogonal arrays. The use of an orthogonal design can significantly reduce the cost and time of the experiment [44,45]. The mixture ratio of HBFC with stable and excellent properties can be selected more accurately by using an analysis of means (ANOM) and variances (ANOVA) [14,28,29].

Here, in order to seek the optimum mixture ratio of HBFCs meeting the performance requirements of modern prefabricated lightweight panels, mix proportions of 16 groups HBFCs were designed with an orthogonal experiment, and the HBFCs were fabricated by the pre-foaming method. The corresponding ρ_d , f_{cu} , and k_c were characterized and analyzed by ANOM and ANOVA, the optimization verification of the mix ratio and economic cost of HBFC were also evaluated.

2. Materials and Methods

2.1. Raw Materials

The HBSC, acquired from Polar Bear Building Material Co., Ltd. (Tangshan, China), was produced with solid waste. Grade-II fly ash (FA) was obtained from the Shandong Huadian power plant (Qingdao, China). The chemical composition and mineral composition of the HBSC clinker and the chemical composition of FA were characterized by X-ray powder diffraction (XRD, D8 Advance type, Bruker Corp., Leipzig, Germany) and an X-ray fluorescence spectrometer (XRF, XRF-1800 type, Shimadzu Corp., Kyoto, Japan), listed in Tables 1 and 2. The composite foaming agent was bought from Guangzhou Haofeng chemical company (Guangzhou, China). The naphthalene-based superplasticizer (NSP) was bought from Shanghai Chenqi chemical company (Shanghai, China). The tap water was used.

Table 1. Chemical compositions and mineral compositions of HBSC.

Chemical Composition	CaO	SiO ₂	Al ₂ O ₃	Fe ₂ O ₃	MgO	SO ₃	TiO ₂	Sum	Loss
	51.54	13.80	15.34	1.52	2.08	14.21	0.71	99.58	0.38
Mineral Composition	C ₄ A ₃ S̄		C ₂ S	f-CaSO ₄	C ₄ AF	f-CaO	CT		
	29.35		38.06	13.64	5.08	1.84	1.11		

Table 2. Chemical compositions of grade-II FA.

Ingredient	SiO ₂	Al ₂ O ₃	Fe ₂ O ₃	CaO	MgO	SO ₃	Na ₂ O	K ₂ O	Loss
FA	54.91	25.82	6.91	8.74	2.05	0.61	0.32	0.10	0.54

2.2. Mix Proportion and Orthogonal Experimental Design

The dosage to binder of FA, water, foam, and the naphthalene-based superplasticizer (w_{FA} , W/B , w_{FOAM} , and w_{NSP}) are the main parameters separately or jointly affecting the physical performances (ρ_d , f_{cu} , and k_c) of HBFC. The mix proportions of FCs were designed using an orthogonal experiment with four parameters w_{FA} , W/B , w_{FOAM} , and w_{NSP} as the main factors. Sixteen different mixtures of HBFCs were prepared by varying (1) FA replacement for HBSC (w_{FA}) from 0 to 20 wt% with a 5 wt% gradient, (2) water to binder ratio (W/B) from 0.40 to 0.55 with a 0.05 gradient, (3) foam fraction of binder (w_{FOAM}) from 13.5 to 16.5 wt% with a 1 wt% gradient, (4) NSP fraction of binder (w_{NSP}) from 0 to 1.0 wt% with a 0.2 wt% gradient.

The k_c of FA is lower than cement, which can improve the thermal insulation of FC, and its pozzolanic effect can improve the long-term strength of FC. The superplasticizer can improve the workability of the fresh FC slurry, reduce the W/B , and eventually improve the f_{cu} of FC. The amount of foam affects the ρ_d and f_{cu} of the FC—the greater the w_{FOAM} , the greater the pore volume and the lower the k_c of the FC. Four levels were taken for each factor, as listed in Tables 3 and 4 [28]. The ρ_d , f_{cu} , and k_c were used as evaluation indicators and the optimal mix ratio was finally achieved by the ANOM and ANOVA methods.

Table 3. Factors and levels on preparation of HBFC.

Level \ Factor	A wFA (wt%)	B W/B	C wFOAM (wt%)	D wNSP (wt%)
1	0	0.40	13.5	0
2	10	0.45	14.5	0.6
3	15	0.50	15.5	0.8
4	20	0.55	16.5	1.0

Table 4. $L_{16}(4^4)$ Orthogonal experimental array on mix proportion of HBFC.

Item No. \ Factor	A_wFA (wt%)	B_W/B	C_wFOAM (wt%)	D_wNSP (wt%)
d_1	0 (1)	0.40 (1)	13.5 (1)	0% (1)
d_2	0 (1)	0.45 (2)	14.5 (2)	0.6% (2)
d_3	0 (1)	0.50 (3)	15.5 (3)	0.8% (3)
d_4	0 (1)	0.55 (4)	16.5 (4)	1% (4)
d_5	10 (2)	0.40 (1)	14.5 (2)	0.8% (3)
d_6	10 (2)	0.45 (2)	13.5 (1)	1% (4)
d_7	10 (2)	0.50 (3)	16.5 (4)	0% (1)
d_8	10 (2)	0.55 (4)	15.5 (3)	0.6% (2)
d_9	15 (3)	0.40 (1)	15.5 (3)	1% (4)
d_{10}	15 (3)	0.45 (2)	16.5 (4)	0.8% (3)
d_{11}	15 (3)	0.50 (3)	13.5 (1)	0.6% (2)
d_{12}	15 (3)	0.55 (4)	14.5 (2)	0% (1)
d_{13}	20 (4)	0.40 (1)	16.5 (4)	0.6% (2)
d_{14}	20 (4)	0.45 (2)	15.5 (3)	0% (1)
d_{15}	20 (4)	0.50 (3)	14.5 (2)	1% (4)
d_{16}	20 (4)	0.55 (4)	13.5 (1)	0.8% (3)

2.3. Preparation Procedures of HBFC

First, the HBSC, FA, and NSP were weighed according to the designed mix ratio and dry-mixed in a rotating mortar mixer (JJ-5 type, Wuxi, China) for 1 min. Then, the weighed water was added into the mixer to prepare the slurry. Meanwhile, the appropriate weight of foam was generated by a foam generator (BL168-8 type, Hefei Baile Energy Equipment Company, Hefei, China) and immediately added to the slurry mixture. The foam was mixed with the slurry and stirred for some time until there was no physical indication of the foam on the surface and all the foam was evenly distributed and incorporated into the mixture [36].

Fresh HBFC slurry was poured into six cubic molds with sizes of $100 \times 100 \times 100 \text{ mm}^3$ and three prism molds with sizes of $300 \text{ mm} \times 300 \text{ mm} \times 60 \text{ mm}$. Unlike a normal concrete casting process, the HBFC slurry should not be subjected to any form of compaction or vibration. The specimens were cast in molds covered with plastic film to prevent moisture loss. Once demolded after 24 h, the specimens were kept in a standard curing room (temperature $22 \pm 2 \text{ }^\circ\text{C}$, relative humidity $\geq 95\%$) up to the day of testing. The schematic fabricating process of HBFC is shown in Figure 1.

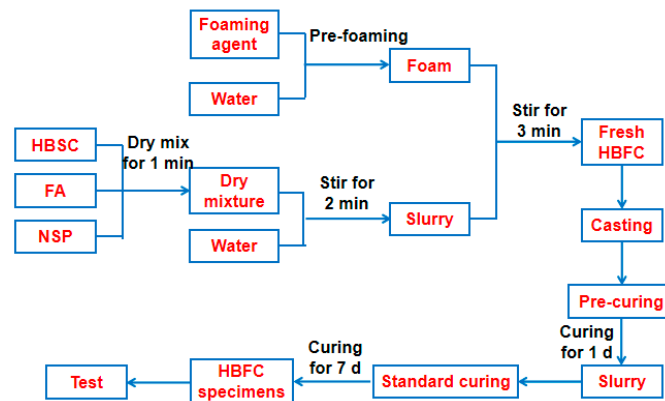


Figure 1. Schematic preparing process of HBFC.

3. Property Characterizations

3.1. Properties of Foam

Taking into consideration the cost of the foaming agent and its foaming performance, it was necessary to select an appropriate dilution ratio to configure the foaming agent solution, which was used to produce HBFC [35]. In this study, the above-mentioned composite foaming agent was used to conduct four tests with varied dilution ratios of 1:10, 1:20, 1:30, and 1:40, respectively, and its foam properties were tested using a foam performance measuring instrument (YJ-1 type, foam tester for FC, Tianjian Instrument Co., Ltd., Cangzhou, China), shown in Figure 2.

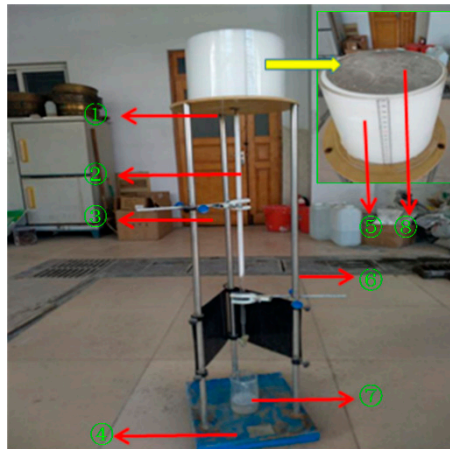


Figure 2. A foam tester for FC: ①, Steel tray; ②, long scale tube; ③, catheter clip; ④, base; ⑤, capacity cylinder (enlarged green square); ⑥, support bar; ⑦, bleeding capacity bottle; ⑧, aluminum plate.

The foam properties were characterized in accordance with criterion JG/T 266-2011 (Beijing, China). The volume of the ⑤capacity cylinder is V_F , and its mass was recorded as m_a after being measured. The foam was directly sprayed into the ⑤capacity cylinder through the aspiration pipe of the foam generator. The excess foam on the top of the ⑤capacity cylinder was scrapped and the total mass of the foam and the ⑤capacity cylinder m_b was weighed. The foam density (ρ_F) can be calculated by Equation (1) and the foamability can be calculated by Equation (2):

$$\rho_F = \frac{m_b - m_a}{V_F} \quad (1)$$

$$M = \frac{V_F}{(m_b - m_a)/\rho} \quad (2)$$

where M is the foamability of the foam, V_F is the volume of the foam, m_b is the total mass of the foam and the capacity cylinder, m_a is the mass of the foam, ρ_F is the foam density, and ρ is the density of the foaming agent solution.

After measuring the ρ_F and M , the capacity cylinder filled with foam was placed on top of the ① steel tray. After 1 h, the 1 h settling distance of foam in the ⑤ capacity cylinder and 1 h bleeding volume of foam in the ⑦ bleeding capacity bottle were recorded as S_v and B_v , respectively. The foam properties of each foam agent dilution ratio were measured 3 times.

3.2. Dry Density

The cubic specimens were weighed after they were dried at 55 ± 5 °C to constant weights within an oven drier (BG2-140 type, vacuum oven, Shanghai Boyi Equipment Factory, Shanghai, China), then the ρ_d of the specimen was calculated from the weight to volume ratio and three duplicates for each group were conducted.

3.3. Compressive Strength

Since the strengths of HBFC were relatively low, these cubic specimens were crushed using a microelectronic control testing machine (YAW-3000 type, Jinan Nusino Industrial Testing System Co., Ltd., Jinan, China) with 1.0 mm/min cross head speed and nearest 0.01 N precision [11], and three duplicates for each group were conducted. The f_{cu} was acquired from Equation (3):

$$f_{cu} = F/A_c \quad (3)$$

where f_{cu} is the compressive strength of the HBFC specimen at 7 d age, F is the maximum failure load, and A_c is the initial pressure area of the test specimen.

3.4. Thermal Conductivity

The k_c of the material is the heat transferred per unit of area and per unit of time when the temperature difference between the two sides is 1 °C under stable heat transfer conditions. Here, the prism HBFC panels (300 mm × 300 mm × 60 mm) were dried at 55 ± 5 °C to a constant weight in order to eliminate the influence of moisture on k_c then polished on both sides to achieve good contacts between specimens and hot (or cold) plates. An automatic double plane thermal conductivity tester (SSX-DR300 type, thermal conductivity measuring instrument, Beijing Sansixing Measurement and Control Technology Co., Ltd., Beijing, China) was employed to measure k_c of HBFC. The HBFC specimen was placed between two plates, the temperatures of the hot and cold plates were set as 40 °C and 20 °C, and the heat flow rate was measured when the equilibrium condition was reached after about 3 h [36]. The temperature difference between hot and cold plates was controlled by a control unit [37]. Three duplicates for each group were examined, and the k_c of the HBFC can be calculated by Equation (4):

$$k_c = \frac{\varphi \times d}{S \times \Delta T} \quad (4)$$

where, k_c is the thermal conductivity (W/m·k), φ is heat flow rate (J/s), d is average thickness of the specimen (m), S is average area of the specimen (m²), and ΔT is temperature difference between the hot and cold plates (°C).

3.5. Macroscopic and Microscopic Observation

The pore sizes, distributions, and pore structure in the macroscopic and microscopic scale of HBFC were observed by a digital camera (EOS 800D type, Canon (China), Beijing, China) and field emission scanning microscope (FEG-SEM, JSM 7500f type, Jeol, Tokyo, Japan), respectively.

4. Results

4.1. Foam Properties

The mean results and deviations of the foam properties of composite foam agents under different dilution ratios are revealed in Table 5. The basic requirements for the performance index of the foam agent can refer to criterion JG/T 266-2011 (Beijing, China), also shown in Table 5.

Table 5. Foam properties of composite foam agents under different dilution ratios.

Dilution Ratio	B_v (mL)	S_v (mm)	M	ρ_F (kg/m ³)
1:10	40.6 ± 2.1	4.7 ± 0.3	35.1 ± 1.2	29.5 ± 0.9
1:20	55.2 ± 2.8	5.4 ± 0.3	29.0 ± 1.6	36.7 ± 1.1
1:30	65.1 ± 3.5	8.0 ± 0.4	27.9 ± 0.9	45.0 ± 1.4
1:40	89.3 ± 4.0	11.5 ± 0.6	23.7 ± 1.4	49.1 ± 1.4
JG/T 266-2011	<80	<10	> 20	-

As shown in Table 5 and Figure 3, the 1 h bleeding volume and the 1 h settling distance were lowest (40.6 ± 2.1 mL and 4.7 ± 0.3 mm) and highest (89.3 ± 4.0 mL and 11.5 ± 0.6 mm) when the dilution ratio was 1:10 and 1:40, respectively. With the increase of dilution ratio, the 1 h bleeding volume and 1 h settling distance of the foam steadily increased, as shown in Figure 3. In fact, as the dilution ratio increased, the water content of the foam liquid membrane also increased and the tenacity of the liquid membrane decreased, cracking and bleeding were thus more likely to occur—resulting in defoaming [43].

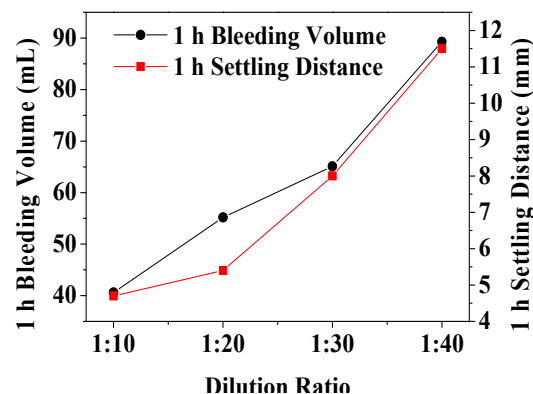


Figure 3. The relationship between 1 h bleeding volume, 1 h settling distance, and dilution ratio.

Foamability was highest (35.1 ± 1.2 times) and lowest (23.7 ± 1.4 times)—and the foam density was the lowest (29.5 ± 0.9 kg/m³) and highest (49.1 ± 1.4 kg/m³)—when the dilution ratio was 1:10 and 1:40, respectively, as demonstrated in Table 5 and Figure 4. With the increase of dilution ratio, foamability gradually decreased and the foam density gradually increased, as shown in Figure 4. Indeed, as the dilution ratio increased, the concentration of the foam solution decreased, resulting in an increase in the surface tension of the liquid and a decrease in the foamability [44,45]. The water content in the foam liquid membrane increased and its density increased accordingly.

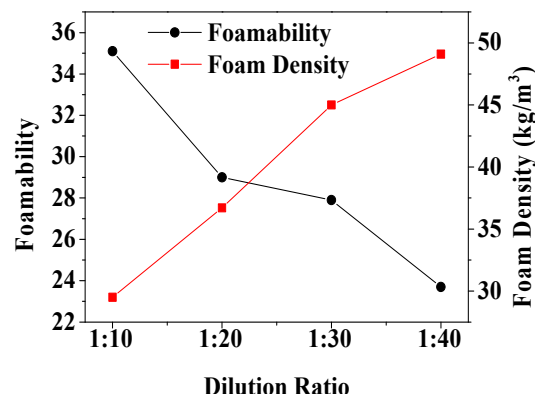


Figure 4. The relationship between foamability, foam density, and dilution ratio.

Thus, considering the cost and performance requirements of composite foam agents, the dilution ratio was selected at 1:30 to produce the foam for HBFC.

4.2. Physical Properties and Orthogonal Range Analysis

The mean results and deviations of the physical properties of 16 groups of HBFCs are revealed in Table 6. An ANOM of the orthogonal test and mix proportion optimization of HBFC are shown accordingly in Table 7.

Table 6. Physical performances of HBFC based on the orthogonal test.

Item No.	ρ_d (kg/m ³)	f_{cu} (MPa)	k_c (W/m·k)
d_1	307.3 ± 3.5	0.49 ± 0.04	0.22368 ± 0.00121
d_2	387.0 ± 4.9	1.05 ± 0.12	0.21544 ± 0.00098
d_3	341.0 ± 5.0	0.82 ± 0.09	0.21098 ± 0.00144
d_4	294.4 ± 5.6	0.73 ± 0.09	0.18131 ± 0.00109
d_5	305.7 ± 4.8	0.67 ± 0.05	0.19903 ± 0.00209
d_6	325.5 ± 7.0	0.63 ± 0.02	0.21098 ± 0.00087
d_7	306.8 ± 3.3	0.47 ± 0.02	0.15835 ± 0.00174
d_8	321.2 ± 4.0	0.73 ± 0.04	0.18920 ± 0.00113
d_9	321.0 ± 2.9	0.62 ± 0.06	0.13561 ± 0.00103
d_{10}	329.7 ± 3.9	0.54 ± 0.01	0.11446 ± 0.00144
d_{11}	339.2 ± 6.5	0.69 ± 0.04	0.12552 ± 0.00069
d_{12}	339.9 ± 7.0	0.59 ± 0.02	0.12001 ± 0.00144
d_{13}	298.0 ± 4.1	0.50 ± 0.02	0.09385 ± 0.00117
d_{14}	322.0 ± 3.3	0.51 ± 0.02	0.10492 ± 0.00069
d_{15}	342.5 ± 4.4	0.65 ± 0.06	0.12837 ± 0.00095
d_{16}	329.1 ± 6.6	0.67 ± 0.04	0.13703 ± 0.00126

From the physical properties and the corresponding ANOM shown in Tables 6 and 7, the optimal mix proportion can be obtained with the primary and secondary factors w_{FOAM} and w_{NSP} , respectively. The optimal ratio to reach the lowest ρ_d is $A_2B_1C_4D_1$ with w_{FA} , W/B , w_{FOAM} , and w_{NSP} as 10 wt%, 0.4, 16.5 wt%, and 0 wt%, respectively.

After ANOM calculations, the order of the factors affecting f_{cu} is obtained, which can be ranked in order of importance as $D > A > C > B$. Finally, optimal mix proportion can be obtained at $A_1B_2C_2D_2$ with the value of four factors as 0 wt%, 0.45, 14.5 wt%, and 0.6 wt%, respectively.

From the ANOM, the optimal level of k_c can be obtained, optimal mix proportion is $A_4B_3C_4D_1$ with w_{FA} , W/B , w_{FOAM} , and w_{NSP} as 20 wt%, 0.5, 16.5 wt%, and 0 wt%, respectively, which can be ranked in order of importance as $A > C > D > B$.

Specific analysis on each indicator is further demonstrated as follows.

Table 7. ANOM of the orthogonal test and optimization of the mix proportion of HBFC.

Index	Factor	A	B	C	D	
ρ_d (kg/m ³)	k_1	332.4	308.0	325.3	319.0	Optimal mix proportion: $A_2B_1C_4D_1$
	k_2	314.8	341.1	343.8	336.4	
	k_3	332.5	332.4	326.3	326.4	
	k_4	322.9	321.2	307.2	320.9	
	Range	17.65	33.05	36.55	17.35	
	Optimal level	2	1	4	1	
f_{cu} (MPa)	Factor order	$C > B > A > D$				Optimal mix proportion: $A_1B_2C_2D_2$
	k_1	0.77	0.57	0.62	0.52	
	k_2	0.63	0.68	0.74	0.74	
	k_3	0.61	0.66	0.67	0.68	
	k_4	0.58	0.68	0.56	0.66	
	Range	0.19	0.11	0.18	0.23	
k_c (W/m·k)	Optimal level	1	2	2	2	Optimal mix proportion: $A_4B_3C_4D_1$
	Factor order	$D > A > C > B$				
	k_1	0.20785	0.16304	0.17430	0.15174	
	k_2	0.18939	0.16145	0.16571	0.15600	
	k_3	0.1239	0.15581	0.16018	0.16537	
	k_4	0.11604	0.15689	0.13699	0.16407	
k_c (W/m·k)	Range	0.09181	0.00723	0.03731	0.01364	Optimal mix proportion: $A_4B_3C_4D_1$
	Optimal level	4	3	4	1	
	Factor order	$A > C > D > B$				

4.3. Effect of Various Factors on Dry Density

The relationship between ρ_d and four factors is shown in Figure 5. Even though the mix proportion of HBFC is designed based on the predetermined ρ_d value of 350 kg/m³, the minimum density can be obtained within this narrow density range. The HBFC has the lowest ρ_d when w_{FA} is 10 wt% because the setting time of the binder just matches the foam stabilization time, which minimizes defoaming [40]. It can be seen from Figure 5 that ρ_d first increased and then decreased with the increase of W/B . With the increase of water, the bubble of the foam gradually tends to be saturated, and much of the foam with thin bubble walls will burst due to the unbearable pressure, resulting in a decrease in the amount of complete foam and an increase in ρ_d . When the water continues to increase however, the burst foam does not continue to increase as the bubbles have already saturated. Water’s participation in the hydration is certain, the extra water will only serve as free water to prop up part of the volume which can be evaporated after drying, thus ρ_d will be reduced. The ρ_d of HBFC also first increased and then decreased with w_{FOAM} . Obviously, the foam made up most of the volume of HBFC, w_{FOAM} was found to be the most influential factor on ρ_d , as revealed from the ANOM in Table 7.

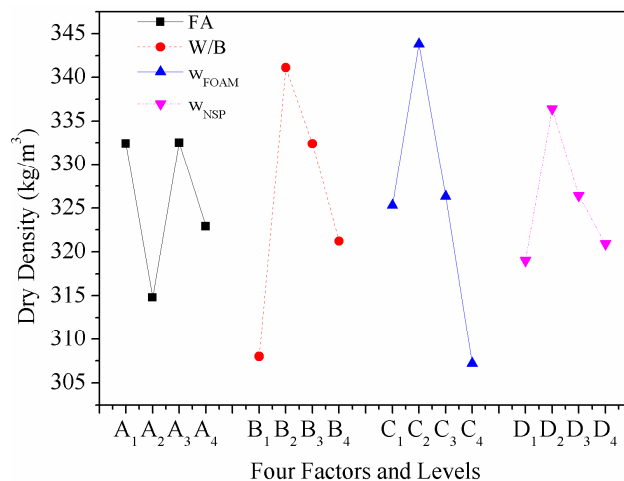


Figure 5. The influence of four factors on the dry density of HBFC.

This phenomenon can be explained by the SEM images of microscopic pore structure in Figure 6. When the w_{FOAM} was 14.5 wt%, the average pore size was smallest within 180 μm and the size distribution was uniform. When the w_{FOAM} was 13.5 wt% and 15.5 wt%, the average pore size was 220 μm and 200 μm , respectively. When the w_{FOAM} was 16.5 wt%, relatively large pores appeared within the largest one of 450 μm and pore sizes differed greatly. The average pore diameter of HBFC first increased and then decreased with the increase of w_{FOAM} , which meant that the pore volume in HBFC first increased and then decreased, resulting in the fluctuating trend of ρ_d with w_{FOAM} [37]. With the increase of w_{NSP} , the ρ_d of HBFC shows a similar fluctuating trend as with w_{FOAM} . As reported, appropriate w_{NSP} can maintain good stability of the foam by improving slurry fluidity, but it will reduce the plastic viscosity of the slurry, resulting in broken air bubbles [37]. When w_{NSP} was 0.6 wt%, only the plastic viscosity of the slurry was reduced, but the fluidity was not effectively improved, which caused a large number of broken bubbles and the ρ_d of HBFC eventually increased. However, the fluidity of the slurry improved and the slurry hardness decreased as w_{NSP} continued to increase, resulting in a decrease in the amount of broken bubbles and a decrease in ρ_d .

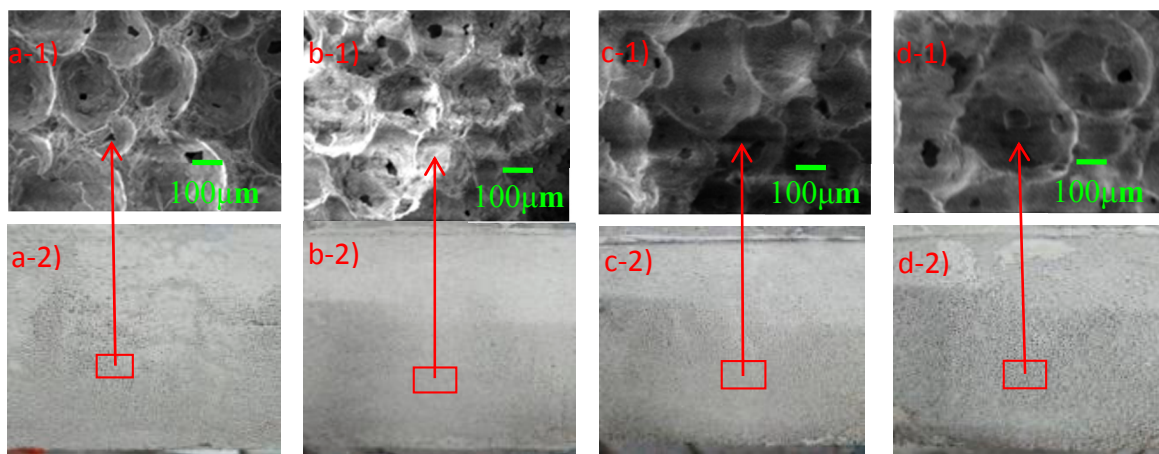


Figure 6. Pore size and naked surface images of HBFC under different w_{FOAM} observed by SEM and digital camera: (a) 13.5 wt%, (b) 14.5 wt%, (c) 15.5 wt%, and (d) 16.5 wt%.

4.4. Effect of Various Factors on Compressive Strength

As shown in Figure 7, the f_{cu} decreased with the increase of w_{FA} . The phenomenon is similar to that of ordinary concrete. The early strength of HBFC is mainly controlled by cement and the 7d strength of HBSC can reach about 90% of its final strength due to its fast hardening and early high strength properties [11].

Thus, the higher the content of HBSC in HBFC, the higher the f_{cu} will be. This rule can also be explained by the microstructure of HBFC—when the binder is only HBSC, the pores of FC are almost closed, there are few connected pores, and the structure of the pore walls is very tight and ductile. With the w_{FA} increase, the number of damaged connected pores tended to increase and the structure of the pore wall gradually became loose, as shown in Figure 8. Thus, f_{cu} decreased as w_{FA} increased.

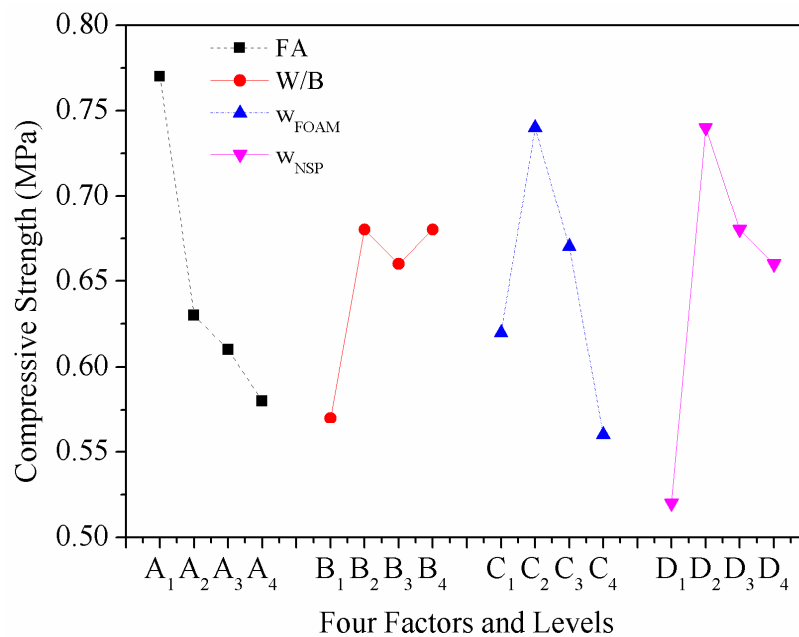


Figure 7. The influence of four factors on the compressive strength of HBFC.

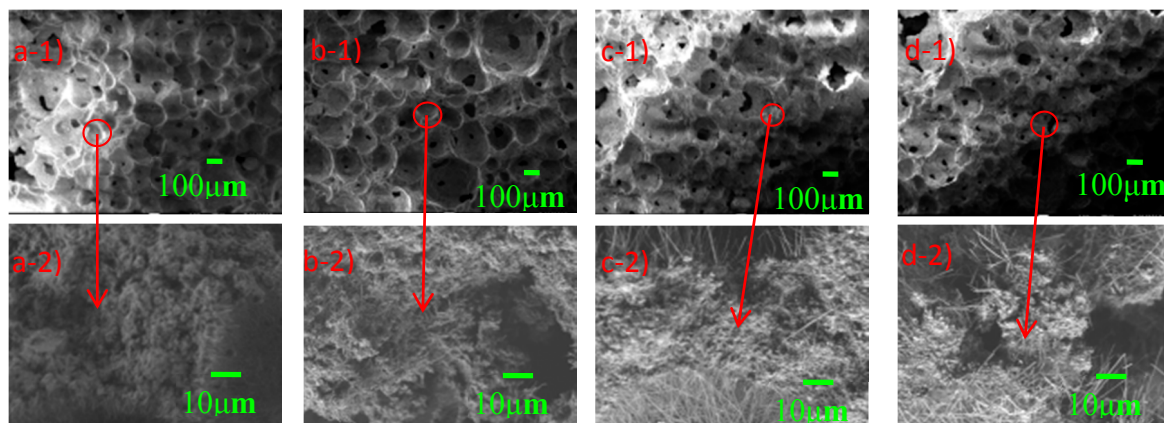


Figure 8. SEM morphology of pore wall structures of HBFC with different w_{FA} : (a) 0 wt%, (b) 10 wt%, (c) 15 wt%, and (d) 20 wt%.

4.5. Effect of Various Factors on Thermal Conductivity

Figure 9 presents the effect of four factors and levels on the k_c of HBFC. Among the four factors, w_{FA} has the most significant influence on k_c , as shown in Table 7 and Figure 9. The k_c shows a significant decline with the increase of w_{FA} . There are two mechanisms on the k_c reduction of FC by adding FA: (1) FA itself has lower k_c than cement; (2) the FA dosage can make the pores in FC more uniform, which is helpful for reducing the k_c [45]. It can be seen from Figure 8 that with the increase of w_{FA} —although the connected holes increase and the pore diameter does not change too much—the pore wall becomes thinner, which makes the pores more compact and increases the porosity. Since the k_c of air is lower than that of other building materials, the higher the porosity, the lower the k_c is. Therefore, based on the above reasons, the k_c of HBFC decreases with the increase of w_{FA} . With the increase in w_{FOAM} , the pore size first decreased and then increased, but the number of close pores when the w_{FOAM} was 14.5 wt% was more than when the w_{FOAM} was 13.5 wt%. Previous researches have reported that porosity accounts for the main volume of FC and that the quality of pores affects the thermal insulation, with larger pore volume and finer pores contributing to better insulation [34,36]. Therefore, in general, with the increase of w_{FOAM} , the k_c of HBFC gradually decreases with the increase

of W/B and w_{NSP} , and the k_c of HBFC arrives to an inflection point, as shown in Figure 7. When the W/B is 0.5 and w_{NSP} is 0.8%, a uniform and stable FC can be obtained, and the bubble can be distributed uniformly and retain stable to a maximum extent, rendering low k_c .

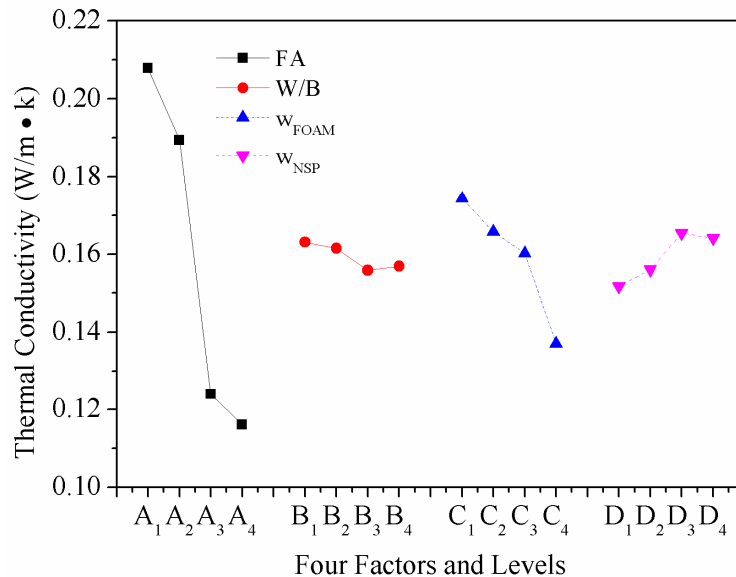


Figure 9. The influence of four factors on the thermal conductivity coefficient of HBFC.

4.6. Analysis of Variances Comprehensive Evaluation on the Optimal Ratio

In order to investigate which factor significantly affects the ρ_d, f_{cu} , and k_c values and select the optimal ratio of HBFC, the ANOVA were studied and the results shown in Table 8.

Table 8. ANOVA results according to ρ_d, f_{cu} , and k_c shown in Tables 4 and 6.

Index	Factor	A	B	C	D	Error
ρ_d (kg/m ³)	DOF	3	3	3	3	3
	SS _i	869.7	2456.6	2674.2	729.1	729.1
	M _i	289.9	818.9	891.4	243.0	243.0
	VR _i	1.19	3.37	3.67	1.00	1.00
f_{cu} (MPa)	DOF	3	3	3	3	3
	SS _i	0.087	0.034	0.070	0.110	0.034
	M _i	0.029	0.011	0.023	0.037	0.011
	VR _i	2.64	1.00	2.09	3.36	1.00
k_c (W/m·k)	DOF	3	3	3	3	3
	SS _i	2.55×10^{-2}	1.47×10^{-4}	3.06×10^{-3}	5.11×10^{-4}	1.47×10^{-4}
	M _i	8.52×10^{-3}	4.89×10^{-5}	1.02×10^{-3}	1.70×10^{-4}	4.89×10^{-5}
	VR _i	174.23 **	1.00	20.86 *	3.48	1.00

Noting that, $F_{0.1}(3,3) = 5.39, F_{0.01}(3,3) = 29.46$; *, ** represent significant, more significant factor, respectively.

The number of levels (4) subtracted by 1 gave the degree of freedom (DOF). The sum of squares (SS_i) is acquired by Equation (5) [25]:

$$SS_i = 4((k_{1i} - k)^2 + (k_{2i} - k)^2 + (k_{3i} - k)^2 + (k_{4i} - k)^2) \quad (5)$$

$(i = A, B, C, D)$

where SS_i stands for the sum of squares and k stands for the 16 mean values. Sum of squares divided by the degree of freedom produced mean squares (M_i).

As demonstrated in Table 8, the minimum mean square ($M_i^{\min} = 243.0$) is chosen as error, other M_i divided by M_i^{\min} gives the variance ratios (VR_i) of ρ_d . Here, because of $1.00 < 1.19 < 3.37 < 3.67 < F_{0.1}(3,3) = 5.39$, the effects of these four factors on ρ_d are not significant, and the order of importance is $C > B > A > D$.

As shown in Table 7 and Figure 5, the difference in ρ_d of HBFC under different factors and levels is little, but when factor A is at level 2, factor B is at level 1, factor C is at level 4, and factor D is at level 1, the minimum ρ_d can be obtained, which are 314.8 kg/m^3 , 308.0 kg/m^3 , 307.2 kg/m^3 , and 319.0 kg/m^3 , respectively.

Consequently, the optimum parameters for ρ_d are w_{FA} at 10 wt%, W/B at 0.4, w_{FOAM} at 16.5 wt%, and w_{NSP} at 0 wt%. As for f_{cu} , the minimum mean square ($M_i^{\min} = 0.011$) is chosen as the error, other M_i divided by M_i^{\min} gives the VR_i of f_{cu} . As $1.00 < 2.09 < 2.64 < 3.36 < F_{0.1}(3,3) = 5.39$, the effects of these four factors on f_{cu} are also not significant, and the order of importance is $D > A > C > B$. From Table 7 & Figure 5, the optimum parameters for f_{cu} can be obtained, which are w_{FA} at 0 wt%, W/B at 0.45, w_{FOAM} at 14.5 wt%, and w_{NSP} at 0.6 wt%. The minimum mean square ($M_i^{\min} = 4.89 \times 10^{-5}$) is chosen as the error, other M_i divided by M_i^{\min} gives the VR_i of k_c . As $20.86 > F_{0.05}(3,3) = 9.28$ and $174.23 > F_{0.01}(3,3) = 29.46$, factor A is the most significant factor on k_c , and factor C is more significant than factors B and D . Similarly, the optimum parameters for f_{cu} can be obtained, which are w_{FA} at 20 wt%, W/B at 0.5, w_{FOAM} at 16.5 wt%, and w_{NSP} at 0 wt%. The optimal solution based on each performance of HBFC is shown in Table 9.

Table 9. Optimal solutions of various factors based on the performance of HBFC.

Performance	Factors and Level			
ρ_d	A_2	B_1	C_4	D_1
f_{cu}	A_1	B_2	C_2	D_2
k_c	A_4	B_3	C_4	D_1

It can be seen from the ANOVA in Table 8, the effect of w_{FA} and w_{FOAM} on the k_c of HBFC is particularly significant. The order of importance of the three performance indicators is $k_c > f_{cu} > \rho_d$. A comprehensive evaluation will be used to seek the optimal proportion for simultaneously satisfying the properties of the three types.

Factor A: For factor A , the optimal levels to satisfy three performances are A_2 , A_1 , and A_4 , respectively, with no overlapping levels as shown in Table 9. The k_c is more important than the other two properties. It can be seen from Table 7, the k_c at A_4 level is $0.11604 \text{ W/m}\cdot\text{k}$, which is better than levels A_1 and A_2 . FA is cheaper than cement and conforms to the concept of green environmental protection. Level A_4 satisfies the requirements of ρ_d and f_{cu} , which are 322.9 kg/m^3 and 0.58 MPa , respectively, as shown in Table 7. After comprehensive consideration, level A_4 ($w_{FA} = 20 \text{ wt\%}$) will be selected.

Factor B: The k_c of level B_3 is $0.15581 \text{ W/m}\cdot\text{k}$, which is better than levels B_1 and B_2 . As shown in Table 7, the f_{cu} of levels B_2 and B_3 are very similar, which are higher than level B_1 . And the ρ_d meet the requirements. Thus, level B_3 ($W/B = 0.5$) is the optimal level.

Factor C: It can be seen from Table 9, there are two performance indicators inclined to level C_4 . The k_c and ρ_d under level C_4 condition are better than C_2 , and the f_{cu} also meets the requirements. Therefore, level C_4 ($w_{FOAM} = 16.5 \text{ wt\%}$) will be selected as the optimal level after comprehensive assessment.

Factor D: As shown in Table 9, there are two performance indicators inclined to level D_1 . But the f_{cu} of level D_2 is 0.74 MPa , which is higher than level D_1 whose f_{cu} is 0.52 MPa , and the k_c of levels D_1 and D_2 is almost equal. The ρ_d under level D_3 also meets the requirement. Hereby, level D_2 ($w_{NSP} = 0.6 \text{ wt\%}$) is selected as the optimal level.

After comprehensive assessment, the optimal proportion of HBFC is ultimately chosen as $A_4B_3C_4D_2$. The verification test demonstrates that, the k_c , f_{cu} , and ρ_d are $0.09234 \pm 0.00142 \text{ W/m}\cdot\text{k}$,

0.58 ± 0.02 MPa, and 293.5 ± 4.9 kg/m³, respectively, which effectively meet the requirements of ultra-light thermal insulation panels.

4.7. Cost and Scalability of HBFC

The raw materials for preparation of HBFC are HBSC, grade-II FA, a composite foaming agent, water, and NSP, and their market prices are 111.7 \$/ton, 14.9 \$/ton, 1,489.4 \$/ton, 0.5 \$/ton, and 4,468.3 \$/ton. The production of 1 m³ HBFC that meets the performance criteria requires 200 kg of HBSC cement, 50 kg of grade-II FA, 6.5 kg of composite foaming agent, 80 kg of water, and 1.5 kg of NSP, and the total cost is about 39.54 \$/m³. As far as we know, the key to make ultra-light FC is to achieve the matching of binder condensation and foam defoaming. If OPC and FA are used to make FC that meets the above requirements for f_{cu} and ρ_d , it is necessary to add an appropriate amount of accelerator and foam stabilizer, with the common-used fractions as 0.3 wt% and 0.6 wt% of the binder. The price of the OPC, accelerator, and foam stabilizer are 74.5 \$/ton, 29,788.5 \$/ton, and 4,468.3 \$/ton, respectively. The total cost of 1 m³ OPC-based FC that meets the properties is about 44.7 \$/m³.

Therefore, both in terms of physical properties and cost, the HBFC has superior advantages and cost-effectiveness than of OPC-based FC, and the pre-foaming method in this study is also helpful to scalability preparation of HBFC.

5. Conclusions

The 1h bleeding volume and 1 h settling distance of the foam increase with the dilution ratio of the foam. The foamability gradually decreases and the foam density gradually increases with the increase of dilution ratio. When the dilution ratio is higher than 1:30, the foam properties can meet the requirements. When the dilution ratio is 1:10, the foam stability is best, with 1 h bleeding volume and 1 h settling distance of the foam as 40.6 ± 2.1 mL and 4.7 ± 0.3 mm, respectively.

The ρ_d shows no regular trend with the change of four factors. In the mixing and curing process, the less the foam is broken, the higher the porosity of HBFC, and the lower the ρ_d of HBFC. In 16 groups of HBFCs, the minimum ρ_d is 294.4 ± 5.6 kg/m³. In general, the higher the ρ_d , the higher the f_{cu} of HBFC. When the pore size of HBFC is small, the pore wall is thick, the connected pores are few, and the pore wall structure is strong, the f_{cu} of HBFC is more favorable. The highest f_{cu} can reach 1.05 ± 0.12 MPa. With the increase of w_{FA} and w_{FOAM} , the porosity of HBFC can be improved, thus significantly reducing the k_c of HBFC. The lowest k_c in 16 groups can reach 0.09385 ± 0.00117 W/m·k.

From ANOM and ANOVA, the order of the factors affecting the ρ_d , f_{cu} , and k_c can be ranked in order of importance as $C > B > A > D$ ($W/B > w_{FOAM} > w_{FA} > w_{NSP}$, $D > A > C > B$, and $A > C > D > B$, respectively). Optimal mix proportion of ρ_d , f_{cu} , and k_c of HBFC based on orthogonal experimental are $A_2B_1C_4D_1$, $A_1B_2C_2D_2$, and $A_4B_3C_4D_1$, respectively.

With the increase in w_{FOAM} , the micropore size increases and the uniformity deteriorates. When the w_{FOAM} is 16.5 wt%, the largest pore diameter can reach 450 μ m, which undoubtedly improves the porosity of HBFC and is beneficial to reduce the ρ_d and k_c of HBFC. With the increase of w_{FA} , the number of connected pores increases and the pore structures become looser, which is bad for the f_{cu} .

Through comprehensive assessment, the optimal mix ratio of HBFC is $A_4B_3C_4D_2$. The k_c , f_{cu} , and ρ_d are 0.09234 ± 0.00142 W/m·k, 0.58 ± 0.02 MPa, and 293.5 ± 4.9 kg/m³, respectively, and the corresponding cost of HBFC is about 39.5 \$/m³.

Future studies will focus on surface water repellent treatment of HBFC, to achieve lower k_c , and effectively meet the thermal insulation requirements of prefabricated ultra-light building panels.

Author Contributions: Methodology, formal analysis, data curation, and writing—original draft, C.L.; conceptualization, supervision, and writing—review and editing, J.L.; visualization and funding acquisition, Q.L.; validation, S.G.; resources, Z.J.; software, S.L.; project administration, P.Z.; investigation, S.C.

Funding: This research was funded by grants from National Natural Science Foundation of China (No. 51878364, 51578297, and 51878366), Natural Science Foundation of Shandong Province (No. ZR2018MEE043 and ZR2017ZC0737), Qingdao Municipal Government Procurement Project (No. 402019201700013), and the National “111” project.

Acknowledgments: This research was funded by grants from National Natural Science Foundation of China (No. 51878364, 51578297, and 51878366), Natural Science Foundation of Shandong Province (No. ZR2018MEE043 and ZR2017ZC0737), Qingdao Municipal Government Procurement Project (No. 402019201700013), and the National “111” project.

Conflicts of Interest: The authors declare no conflict of interest.

Abbreviations

The following abbreviations are used in this manuscript:

FC	Foam concrete
HBSC	High-belite sulphoaluminate cement
HBFC	HBSC-based FC
OPC	Ordinary Portland cement
FA	Fly ash
PP	Polypropylene fiber
CNT	Carbon nanotube
SDS	Sodium dodecyl sulfate
SAC	Sulphoaluminate cement
ANOM	Analysis of means
ANOVA	Analysis of variances
NSP	Naphthalene-based superplasticizer
W/B	Water-binder ratio
DOF	Degree of freedom
VR	Variance ratio

References

- Hung, M.K.; Johnson, A.U.; Zamin, J.M. Bond properties of lightweight concrete—A review. *Constr. Build. Mater.* **2016**, *112*, 478–496.
- Ma, C.; Chen, B. Properties of foamed concrete containing water repellents. *Constr. Build. Mater.* **2016**, *124*, 106–114. [[CrossRef](#)]
- Huang, Z.; Zhang, T.; Wen, Z. Proportioning and characterization of Portland cement-based ultra-lightweight foam concretes. *Constr. Build. Mater.* **2015**, *79*, 390–396. [[CrossRef](#)]
- Jones, M.R.; Mc Carthy, A. Preliminary views on the potential of foamed concrete as a structural material. *Mag. Concr. Res.* **2005**, *57*, 21–31. [[CrossRef](#)]
- Chen, B.; Liu, J.Y. Properties of lightweight expanded polystyrene concrete reinforced with steel fiber. *Cem. Concr. Res.* **2004**, *34*, 1259–1263. [[CrossRef](#)]
- Ali, S.A.; Juan, T.V.; Thomas, N.R.; Charles, C.G. Effects of expanded polystyrene (EPS) particles on fire resistance, thermal conductivity and compressive strength of foamed concrete. *Constr. Build. Mater.* **2016**, *112*, 716–724.
- Chen, B.; Zhen, W. Experimental research on properties of high-strength foamed concrete. *J. Mater. Civil Eng.* **2012**, *32*, 240–246.
- Zhang, P.; Hou, D.S.; Liu, Q.; Liu, Z.L.; Yu, J. Water and chloride ions migration in porous cementitious materials: An experimental and molecular dynamics investigation. *Cem. Concr. Res.* **2017**, *102*, 161–174. [[CrossRef](#)]
- Ma, C.; Chen, B. Properties of a foamed concrete with soil as filler. *Constr. Build. Mater.* **2015**, *76*, 61–69.
- Tikalsky, P.J.; Pospisil, J.; MacDonald, W. A method for assessment of the freeze–thaw resistance of preformed foam cellular concrete. *Cem. Concr. Res.* **2004**, *34*, 889–893. [[CrossRef](#)]
- Kunhanandan Nambiar, E.K.; Ramamurthy, K. Influence of filler type on the properties of foam concrete. *Cem. Concr. Compos.* **2006**, *28*, 475–480. [[CrossRef](#)]

12. Weigler, H.; Karl, S. Structural lightweight aggregate concrete with reduced density-lightweight aggregate foamed concrete. *Int. J. Cem. Compos. Lightweight. Concr.* **1980**, *2*, 101–104. [[CrossRef](#)]
13. Mydin, M.A.O.; Wang, Y.C. Structural performance of lightweight steel-foamed concrete-steel composite walling system under compression. *J. Steel. Constr.* **2011**, *49*, 66–76.
14. Luo, J.L.; Hou, D.S.; Li, Q.Y.; Wu, C.F.; Zhang, C.W. Comprehensive performances of carbon nanotube reinforced foam concrete with ethyl silicate impregnation. *Constr. Build. Mater.* **2017**, *131*, 512–516. [[CrossRef](#)]
15. Kearsley, E.P.; Wainwright, P.J. The effect of high fly ash content on the compressive strength of foamed concrete. *Cem. Concr. Res.* **2001**, *31*, 105–112. [[CrossRef](#)]
16. Berry, E.E.; Hemmings, R.T.; Zhang, M.H.; Cornelius, B.J.; Golden, D.M. Hydration in high-volume fly ash concrete binders. *ACI Mater. J.* **1994**, *91*, 382–389.
17. Ramamurthy, K.; Kunhanandan Nambiar, E.K.; Indu Siva Ranjani, G. A classification of studies on properties of foam concrete. *Cem. Concr. Compos.* **2009**, *31*, 388–396. [[CrossRef](#)]
18. Stuart, K.D.; Anderson, D.A.; Cady, P.D. Compressive strength studies on Portland cement mortars containing fly ash and superplasticizers. *Cem. Concr. Res.* **1980**, *10*, 823–832. [[CrossRef](#)]
19. Wang, Y.; Cao, Y.; Zhang, P.; Ma, Y.; Zhao, T.; Wang, H.; Zhang, Z. Water absorption and chloride diffusivity of concrete under coupling effect of uniaxial compressive load and freeze-thaw cycles. *Constr. Build. Mater.* **2019**, *209*, 566–576. [[CrossRef](#)]
20. Jasinski, R.; Drobiec, L.; Mazur, W. Validation of selected non-destructive methods for determining the compressive strength of masonry units made of autoclaved aerated concrete. *Materials* **2019**, *12*, 389. [[CrossRef](#)]
21. Lee, H.S.; Ismail, M.A.; Woo, Y.J.; Min, T.B.; Choi, H.K. Fundamental study on the development of structural lightweight concrete by using normal coarse aggregate and foaming agent. *Materials* **2014**, *7*, 4536–4554. [[CrossRef](#)] [[PubMed](#)]
22. Lai, Z.Y.; Hu, Y.; Fu, X.J.; Lu, Z.Y.; Lv, S.Z. Preparation of porous materials by magnesium phosphate cement with high permeability. *Adv. Mater. Sci. Eng.* **2018**, *12*, 5910560.
23. Amran, Y.H.M.; Farzadnia, N.; Ali, A.A.A. Properties and applications of foamed concrete—A review. *Constr. Build. Mater.* **2015**, *101*, 990–1005. [[CrossRef](#)]
24. Karl, S.; Woerner, J.D. *Foamed Concrete-Mixing and Workability, Workability of Special Fresh Concretes*; Chapman and Hall: London, UK, 1994; p. 217.
25. Zulkarnain, F.; Ramli, M. Durability of performance foamed concrete mix design with silica fume for housing development. *J. Mater. Sci. Eng.* **2011**, *5*, 518–527.
26. Kearsley, E.P.; Wainwright, P.J. The effect of porosity on the strength of foamed concrete. *Cem. Concr. Res.* **2002**, *32*, 233–239. [[CrossRef](#)]
27. Khan, M.I. Experimental Investigation on Mechanical Characterization of Fiber Reinforced Foamed Concrete. Master's Thesis, University of Akron, Akron, OH, USA, 2014.
28. Luo, J.L.; Li, Q.Y.; Zhao, T.J.; Gao, S.; Sun, S.W.; Chen, L. Thermal and electrical resistances of carbon nanotube-reinforced foamed concrete. *Nanosci. Nanotech. Lett.* **2014**, *6*, 72–79. [[CrossRef](#)]
29. Yakovlev, G.; Keriene, J.; Gailius, A.; Girniene, I. Cement based foam concrete reinforced by carbon nanotubes. *Mater. Sci.* **2006**, *12*, 147–151.
30. Szelag, M. Mechano-physical properties and microstructure of carbon nanotube reinforced cement paste after thermal load. *Nanomaterials* **2017**, *7*, 267. [[CrossRef](#)]
31. Sun, C.; Zhu, Y.; Guo, J.; Zhang, Y.M.; Sun, G.X. Effects of foaming agent type on the workability, drying shrinkage, frost resistance and pore distribution of foamed concrete. *Constr. Build. Mater.* **2018**, *186*, 833–839. [[CrossRef](#)]
32. Sugama, T.; Brothers, L.E.; Putte, T.R.V.D. Air-foamed calcium aluminate phosphate cement for geothermal wells. *Cem. Concr. Compos.* **2005**, *27*, 758–768. [[CrossRef](#)]
33. Lim, S.K.; Tan, C.S.; Li, B.; Ling, T.C.; Hoaaain, M.U.; Poon, C.S. Utilizing high volumes quarry wastes in the production of lightweight foamed concrete. *Constr. Build. Mater.* **2017**, *151*, 441–448. [[CrossRef](#)]
34. Mounanga, P.; Gbongbon, W.; Poullain, P.; Turcry, P. Proportioning and characterization of lightweight concrete mixtures made with rigid polyurethane foam wastes. *Cem. Concr. Compos.* **2008**, *30*, 806–814. [[CrossRef](#)]
35. Zhang, B.Y.; Poon, C.S. Use of furnace bottom ash for producing lightweight aggregate concrete with thermal insulation properties. *J. Clean. Prod.* **2015**, *99*, 94–100. [[CrossRef](#)]
36. Zhang, Z.H.; Provia, J.L.; Reid, A.; Wang, H. Mechanical, thermal insulation, thermal resistance and acoustic absorption properties of geopolymer foam concrete. *Cem. Concr. Compos.* **2015**, *62*, 97–105. [[CrossRef](#)]

37. Jiang, J.; Lu, Z.Y.; Niu, Y.H.; Li, J.; Zhang, Y.P. Study on the preparation and properties of high-porosity foamed concretes based on ordinary Portland cement. *Mater. Des.* **2016**, *92*, 949–959. [[CrossRef](#)]
38. Li, M.; Wu, Z. Orthogonal experimental study on the aerated concrete basing on the compressive strength. *Cem. Wapno Beton* **2011**, *16*, 115–119.
39. Li, Y.; Chen, B. New type of super-lightweight magnesium phosphate cement foamed concrete. *J. Mater. Civ. Eng.* **2015**, *27*, 04014112.
40. Luo, J.L.; Zhu, G.X.; Zhang, F.F.; Li, Q.Y.; Zhao, T.J.; Zhu, X.Q. Orthogonal experimentation for optimization of TiO₂ nanoparticles hydrothermal synthesis and photocatalytic property of TiO₂/concrete composite. *RSC Adv.* **2015**, *5*, 6071–6078. [[CrossRef](#)]
41. Wu, X.; Leung, D.Y.C. Optimization of biodiesel production from camelina oil using orthogonal experiment. *Appl. Energ.* **2011**, *88*, 3615–3624. [[CrossRef](#)]
42. Martin, A.; Grolle, K.; Bosh, M. Network foaming properties of various proteins adsorbed at the air/water interface in relation to foam stability. *Colloid Interface Sci.* **2002**, *254*, 175–183. [[CrossRef](#)]
43. Kramer, C.; Schauerte, M.; Kowald, T.L.; Trettin, R.H.F. Three-phase-foams for foam concrete application. *Mater. Charact.* **2015**, *102*, 173–179. [[CrossRef](#)]
44. Tarameshloo, A.; Kani, E.N.; Allahverdi, A. Performance evaluation of foaming agents in cellular concrete based on foamed alkali-activated slag. *Can. J. Civ. Eng.* **2017**, *44*, 893–898. [[CrossRef](#)]
45. Lazniewska-Piekarczyk, B.; Szwabowski, J. The Influence of the type of anti-foaming admixture and superplasticizer on the properties of self-compacting mortar and concrete. *J. Civ. Eng. Manag.* **2012**, *18*, 408–415. [[CrossRef](#)]



© 2019 by the authors. Licensee MDPI, Basel, Switzerland. This article is an open access article distributed under the terms and conditions of the Creative Commons Attribution (CC BY) license (<http://creativecommons.org/licenses/by/4.0/>).